Role of S-turn2 in the Structure, Dynamics, and Function of Mitochondrial Ribosomal A-Site. A Bioinformatics and Molecular Dynamics Simulation Study

Joanna Panecka,[†,‡] Marek Havrila,[¶,§] Kamila Réblová,[¶] Jiří Šponer,*[,¶,§] and Joanna Trylska*[,‖]

[†]Department of Biophysics, Institute of Experimental Physics and [‖]Centre of New Technologies, University of Warsaw, Żwirki i Wigury 93, 02-089 Warsaw, Poland
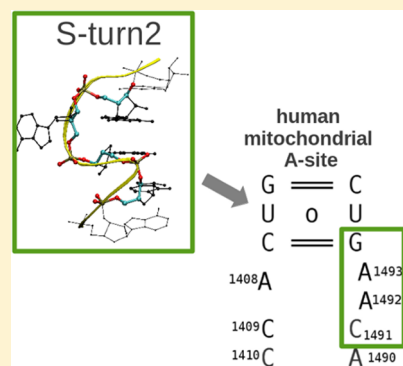
[‡]Interdisciplinary Centre for Mathematical and Computational Modelling, University of Warsaw, Pawińskiego 5a, 02-106 Warsaw, Poland

[¶]CEITEC − Central European Institute of Technology, Masaryk University, Campus Bohunice, Kamenice 5, 625 00 Brno, Czech Republic

[§]Institute of Biophysics, Academy of Sciences of the Czech Republic, Královopolská 135, 612 65 Brno, Czech Republic

Ⓢ *Supporting Information*

ABSTRACT: The mRNA decoding site (A-site) in the small ribosomal subunit controls fidelity of the translation process. Here, using molecular dynamics simulations and bioinformatic analyses, we investigated the structural dynamics of the human mitochondrial A-site (native and A1490G mutant) and compared it with the dynamics of the bacterial A-site. We detected and characterized a specific RNA backbone configuration, S-turn2, which occurs in the human mitochondrial but not in the bacterial A-site. Mitochondrial and bacterial A-sites show different propensities to form S-turn2 that may be caused by different base-pairing patterns of the flanking nucleotides. Also, the S-turn2 structural stability observed in the simulations supports higher accuracy and lower speed of mRNA decoding in mitochondria in comparison with bacteria. In the mitochondrial A-site, we observed collective movement of stacked nucleotides A1408·C1409·C1410, which may explain the known differences in aminoglycoside antibiotic binding affinities toward the studied A-site variants.

■ INTRODUCTION

The translation of mRNA to produce functional proteins is one of the key processes of life, whose main principles are conserved among all living organisms. Translation is catalyzed by ribosomes—assemblies of RNA and proteins which are composed of two subunits, small and large. The ribosomal aminoacyl tRNA binding site (mRNA decoding site, A-site), located in the small ribosomal subunit, at the stem of the long h44 helix, is responsible for the fidelity of (mRNA codon)−(tRNA anticodon) recognition. In particular, two mobile adenines, 1492 and 1493, (according to *E. coli* sequence numbering) in the A-site are the most important components of the molecular switch that controls accuracy of mRNA decoding. They flip in and out from the rRNA internal loop in h44 helix, through its minor groove,[1,2] being in a state of dynamic equilibrium slightly shifted toward the flipped-in configuration in the absence of tRNA[3,4] The binding of an mRNA codon and tRNA anticodon during translation requires a flipped-out state of these flexible adenines,[5] whereas in the flipped-in state, the A-site is inactive. The flipped-out adenines create a precise net of hydrogen bonds with mRNA and A-site–tRNA, which ensures sufficient stabilization of the complex only in the case of the correct codon−anticodon pair.[6] The effectiveness of decoding depends on the adenine flipping

movement and must be a compromise between the speed (i.e., efficiency) and accuracy.

The sequences and also overall secondary structures of A-site forming rRNAs are to large extent conserved among prokaryotes and eukaryotes.[7] For instance, the sequences of *E. coli* and *H. sapiens* mitochondrial decoding sites differ only by three nucleotides (1410, 1490, and 1491 according to *E. coli* numbering) next to the A-site internal loop (Figure 1). However, even point mutations can distort the A-site conformation and affect the dynamics of adenines, as has been previously shown by us.[8] Therefore, it is not surprising that tertiary structures of A-site variants are different.[9]

Moreover, the differences in the A-site sequence affect the selectivity of aminoglycoside antibiotics.[10−12] The 2-deoxy-streptamine aminoglycosides, clinically used antibacterials, bind to the bacterial A-site with relatively high affinities[13] and perturb the mRNA decoding mechanism.[14] These compounds shift the dynamic equilibrium of the adenines 1492 and 1493 to the flipped-out states, enforcing conformations favorable for tRNA anticodon acceptance.[14−19] This causes miscoding
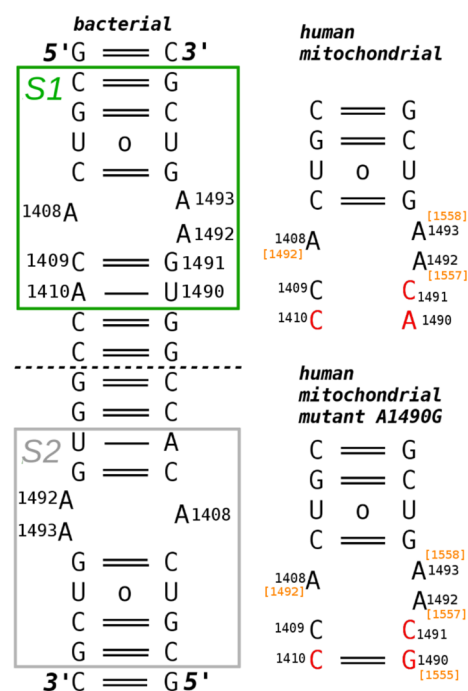
Figure 1. Secondary structures of the models of the simulated A-sites variants. Left: the bacterial sequence (PDB: 3BNL) with two mirrored A-sites *S1* (green) and *S2* (gray). Top right: human mitochondrial native sequence (PDB: 3BNN). Bottom right: human mitochondrial A1490G mutant (PDB: 3BNP). Sequence differences between the bacterial and human mitochondrial A-site are highlighted in red. The original nucleotide numbering as in human mitochondrial ribosomes is in orange.

to be related to aminoglycoside ototoxicity, which can lead to irreversible deafness.[21] Susceptibility to these side effects in some patients was linked to certain mutations in the mitochondrial A-site rRNA sequence (such as A1490G, considered in this work), which lead to creation of additional canonical base pair neighboring with A1492 (see Figure 1).[22] Experimental studies show that these mutations significantly increase the binding of aminoglycosides to the A-site in mitochondrial ribosomes, which results in miscoding and inhibition of translation.[10]

The dynamics of bacterial A-site and its interactions with aminoglycosides have been investigated in many experimental works.[17−19,23−26] Also, there are many computational investigations with molecular dynamics (MD)[8,27−30] and replica exchange MD[3,4] simulations which elucidated the dynamics of A1492 and A1493 in the bacterial A-site. The Poisson–Boltzmann model was also applied to estimate the binding affinities of aminoglycoside antibiotics.[13] Finally, docking[31] and combined virtual screening with 3D-QSAR[32] were used to design new aminoglycoside derivatives. However, so far, the mobility of the human mitochondrial A-site has not been computationally investigated.

Therefore, our aim was to describe and compare the structural and physicochemical properties of the noncomplexed bacterial and human mitochondrial A-sites. We attempted to identify the features of the mRNA decoding site that account for the non-negligible affinity of aminoglycosides toward the human target in mitochondria. To compare the backbone configuration and dynamics of the ribosomal decoding site, we performed MD simulations of different variants of the bacterial and human A-site: (i) of *Escherichia coli* (as a reference), (ii) human mitochondrial, and (iii) human mitochondrial mutant (A1490G). We also conducted sequence analyses to get an overview of sequence variability of ribosomal A-site in different phylogenetic domains.

■ METHODS

Nomenclature. Table 1 lists the performed MD simulations. Throughout this work, we use the following

leading to the production of incorrect proteins, which in the end is lethal to bacterial cells. Promiscuity of aminoglycoside binding results in insufficient selectivity of those antibiotics between human and bacterial decoding sites.[20] In particular, unwanted binding of aminoglycosides to the human mitochondrial A-site has serious consequences for humans. The complexation of these antibiotics with that target was found

Table 1. List of MD Simulations

variant	PDB code	no.	simulation time (ns)	restraints on termini	other
			double A-site models		
E. coli	3BNL	1	300	+	label: *BACT*
H.s. mito.	3BNN	2	300	+	label: *MITO*
H.s. mito. A1490G	3BNP	3	300	+	label: *MITO_MUT*
H.s. mito. A1490G	3BNP	4	100	−	
H.s. mito. A1490G	3BNS	5	300	+	label: *MITO_MUT2*
			single A-site models		
H.s. mito.	3BNN	6	1000	−	
H.s. mito. A1490G	3BNR	7	1000	−	with S-turn2
H.s. mito. A1490G	3BNR	8	1000	−	no S-turn2
			single strands		
H.s. mito.	3BNN	9	500	−	with S-turn2 (run 1)
H.s. mito.	3BNN	10	170	−	with S-turn2 (run 2)
H.s. mito.	3BNN	11	120	−	with S-turn2
H.s. mito.	3BNN	12	480	−	A-form
H.s. mito. A1490G	3BNP	13	470	−	with S-turn2

The abbreviation *H. s.* stands for *Homo sapiens*. Labels of the chosen simulations used throughout the text are also listed.
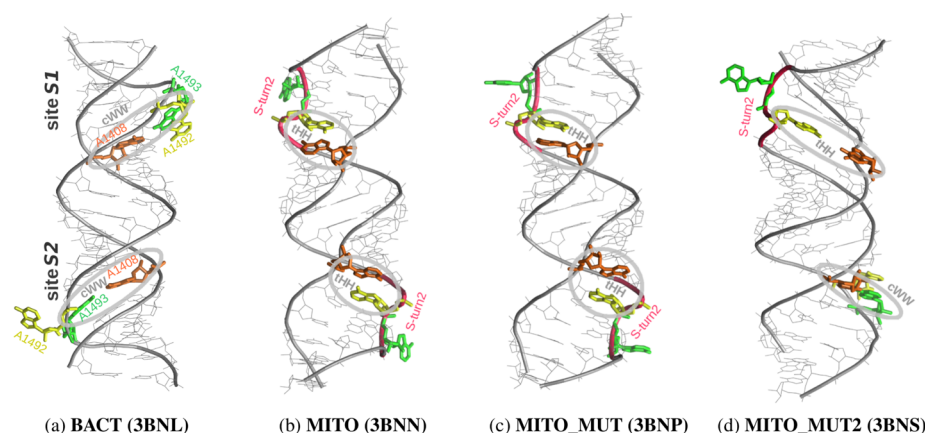
Figure 2. Crystallographic structures of the double A-site models used in this study with PDB codes in parentheses: (a) bacterial, (b) human mitochondrial, (c) human mitochondrial A1490G mutant with C1411:G1489, and (d) human mitochondrial mutant A1490G mutant with U1411:A1489. Gray circles and labels indicate the type of base pairing (for abbreviations, see Methods). The S-turn2 backbone shape is colored magenta, A1492 − yellow, A1493 − green, and A1408 − orange.

names for the main set of the simulations of double A-site models, that is, double-stranded RNA constructs containing two A-sites (see sequences in Figure 1): (i) *BACT* − bacterial, (ii) *MITO* − human mitochondrial, (iii) *MITO_MUT* − human mitochondrial A1490G mutant and (iv) *MITO_MUT*2 − similar to *MITO_MUT*, but with C1411:G1489 base pair mutated to U:A. The two sites in the double A-site crystal model are denoted *S1* and *S2*, as shown in Figure 2. For simplicity, we used *E. coli* numbering of nucleobases also in the human mitochondrial A-site variants; however, original numbering is also shown in Figure 1.

System Selection, Construction, and Starting Conformations. As starting configurations for our MD study, we took crystallographic double-stranded oligoribonucleotide models containing two equivalent (but crystallographically distinct) A-sites (see Figure 1), marked as *S1* and *S2*. The identical binding mode of aminoglycosides in the crystal structures of full ribosomes and in these A-site constructs validates the use of such models.[15,33] These A-site constructs have been previously used in a few computational studies.[3,4,8,27,29,30] The basic characteristics of the crystal structures taken for our study is given in Table S1 (Supporting Information), and most of the starting structures are shown in Figure 2. The adenines 1492/93 adopt various conformations in these A-site models (Figure 2). In site *S2* of the bacterial initial structure (PDB: 3BNL), only A1492 is in a flipped-out conformation, although both adenines are flipped-in in *S1*. In the human mitochondrial variants, native (PDB: 3BNN) and one model of the A1490G mutant (PDB: 3BNP), A1492 in both A-sites is locked outside the RNA internal loop with the backbone forming the so-called "S-turn2" configuration (described in detail later). In the second crystal structure of the mutant which we used (PDB: 3BNS, Figure 2d), a similar locked-out conformation is observed in one site, whereas in the other site A1492 and A1493 are flipped-in, which is similar to the site *S1* of the bacterial model. We should also note that in all these structures, the extra-helical A1492/93 are involved in crystal packing interactions.

In RNA duplexes containing two A-sites, the terminal nucleotides were deleted so that each our model contained 21 nucleotides in each strand (Figure 1). We also carried out some simulations with just a single A-site; in these simulations, we used one of the mirror A-sites (residues 1406−1410 and 1490−

1495) with three additional flanking canonical base pairs at each side of the A-site internal loop. We also simulated single-stranded systems, by subtracting nucleotides 1488−1497 from the X-ray structure. Details of the MD-simulated systems are given in Table 1.

The 5-bromo-uridine in the initial structure for the *MITO_MUT*2 simulation (PDB code: 3BNS[9]) was modified to uridine. Crystal water molecules were not included. Hydrogen atoms were added using the *tleap* program (AmberTools1.5[34]) and optimized in vacuo with *sander* (Amber10 package[35]) with 8000 steps of steepest descent algorithm followed by 2000 steps of conjugate gradient energy minimization. In the next step, each solute molecule was immersed in a truncated octahedral cell of explicit water with a solvent layer of 10−12 Å. The K$^+$ ions were added at the positions of electrostatic potential minima using *tleap* to neutralize the systems.

Positional Restraints. The A-site is a part of the longer rRNA helix 44, which is structurally stable and is stiffened by its participation in ribosomal intersubunit bridges.[36] Further, excessive end-fraying is a potential problem in contemporary simulations of nucleic acids.[37] Thus, in order to partially mimic the condition of helix 44, weak positional restraints of 0.35 kcal/mol/Å^2 were applied to the atoms of the termini at each end of the RNA duplex in some but not all MD simulations of the duplexes' systems (for details, see Table 1). This eliminates end-fraying and also prevents excessive bending of the RNA duplex. Our simulations performed with and without restraints show mostly identical dynamics, even though we found an exception; in the single A-site simulation of the mitochondrial mutant (no. 8 in Table 1) the C1407:G1494 base pair broke at about 150 ns and remained unpaired until the end of the 1 μs trajectory. Therefore, in the current work, we primarily show the results from the simulations with weak positional restraints on the RNA termini (Table 1), albeit the remaining trajectories were also analyzed and provide consistent results.

Molecular Dynamics Conditions, Protocol, and Force Field. All MD simulations were performed in NpT ensemble at 300 K (Berendsen weak coupling algorithm with a time constant of 1.0 ps) and 1 atm pressure (relaxation time of 1.0 ps) with *sander* and *pmemd* modules of the Amber10 and Amber12 package. We used periodic boundary conditions and the particle mesh Ewald (PME) method[38] with a 9 Å cutoff for

long-range interactions. The SHAKE algorithm[39] was applied to all hydrogens to remove their vibrations and enable a longer, 2 fs time step. Center-of-mass motion was removed every 5 ps. The simulation protocol used in this study was previously extensively tested in other studies.[28,40,41] The first stage was minimization of the solvent (1000 steps) followed by linear increasing of temperature from 100 to 300 K (100 ps) with 25 kcal/mol/Å^2 restraints applied to the solute. Then, five short rounds of alternate stages of minimization and 50 ps MD runs were performed with gradual reduction of restraints applied to the solute (5, 4, 3, 2, and 1 kcal/mol/Å^2) and finally 50 ps following runs with 0.5 kcal/mol/Å^2 restraints and without the restraints on the solute. The production phase of each MD simulation lasted 100−1000 ns with the total length of the simulations accumulating to about 6.1 μs.

All simulations are done with the current default bsc0χ_{OL3} version of the Cornell et al. force field.[42−44] χ_{OL3} correction is essential to prevent "ladder" degradation of RNA helices in long simulations.[45] For an overview of nucleic acids force fields, see ref 46. We used K$^+$ cations assigning the parameters of Dang et al.[47] (a radius of 1.87 Å and well depth of −0.1000 kcal/mol) together with SPC/E[48] water model.

Analysis of Molecular Dynamics Data. The data from the production phase of each trajectory, saved each 10 ps, were used for further processing. Analysis of MD simulations was performed mostly with the *ptraj* program from Amber-Tools1.5[34] to extract geometric parameters like angles and distances and to calculate root-mean-square fluctuations (RMSFs). Unless otherwise noted, RMSF calculations were limited to non-hydrogen atoms. Additional analyses were done using in-house Python, Perl, and MATLAB scripts. The plots were generated with gnuplot (http://www.gnuplot.info/) and the MD trajectories were visualized with VMD (http://www.ks.uiuc.edu/Research/vmd/).

The data were clustered with the agglomerative k-means method (implemented in MMTSB Toolset, http://mmtsb.org/) that divides a set of conformations into separate clusters. We used the Cartesian coordinate root-mean-square deviation (RMSD) as a clustering criterion so we obtained a specific number of clusters that satisfied the required RMSD criterion. We may roughly associate the number of the resulting clusters with the conformational variability of the systems. Our MD trajectories were clustered based on the heavy atoms of residues 1490−1493 and 1408−1410 (see nucleotide sequences in Figure 1) in one or the other A-site, with a 2.5 Å RMSD criterion, after initial superposition of the clustered atom subset.

Nucleobase stacking was estimated on the basis of the distance between the centers of mass of the nucleic bases, with the distance criterion of 5.0 Å. Hydrogen bond (H-bond) occupancies were calculated with *ptraj* using a 3.5 Å cutoff for the distance and 120° for the dihedral angle (H-donor)−hydrogen−(H-acceptor). We used Leontis[49] classification of RNA base pairs to characterize the observed nucleotide conformations. The following abbreviations describing the configurations of nucleotides were used: (i) sugar edge − "S", (ii) Hoogsteen edge − "H", and (iii) Watson−Crick edge − "W". For example, *trans* Hoogsteen/sugar-edge configuration was denoted as tHS and *cis* Watson−Crick/Watson−Crick base pair as cWW.

Bioinformatics Analysis. To compare the bacterial and eukaryotic mitochondrial A-sites at the level of their primary structure, the rRNA alignments from Comparative RNA Web Site and Project (http://www.rna.ccbb.utexas.edu; accessed

September 25, 2013)[7] were analyzed. We used in-house scripts to get the nucleotide frequencies at positions of our interest and analyzed the relations with adjacent nucleotides. WebFR3D,[50] the online version of the FR3D[51] program, was used to search for the S-turn2 conformation in RNA X-ray structures. FR3D enables searching in the PDB database using symbolic, geometric, or mixed approaches. We confined the search to a nonredundant set of RNA X-ray structures (release 1.29 at 4.0 Å resolution[52]). One needs to know a common characteristic of a target structure to define the input for symbolic searches. Because we did not have such information about S-turn2, we used a geometric approach with few symbolic restraints. Our aim was to search for all occurrences of S-turn2 conformation in RNA X-ray structures and to evaluate their sequence restraints and context in which this conformation occurs. We performed five different searches (see Table S2 in Supporting Information). Next, we extended the searches by a manual search of the homologous positions in the ribosomes and evaluated the sequence conservation of ribosomal S-turn2. Finally, we used the Molprobity server (http://molprobity.biochem.duke.edu/[53]) to extract the RNA backbone conformational details of the analyzed crystal structures. The backbone suites defined by Richardson et al.[54] were used to characterize the RNA conformations based on the consecutive backbone torsional angles $\delta\epsilon\zeta\alpha\beta\gamma\delta$. The suites are discrete families of conformers observed in the experimental data and correspond to distinct, often functionally important local topologies of RNA backbone. Each family is denoted by a two-character name, for instance, "**1a**" is the canonical (A-form) backbone conformation, whereas "**5z**" is a specific conformation occurring in S-turns. We use this terminology to describe the S-turn2 backbone conformation. Additionally, the classification of Sarver et al.[51] was used to characterize stacking between nucleobases. For instance, the base stacking is classified as "35" when it involves "typical" 3′ side of one nucleobase and 5′ side of the other. The above classification is supplemented by a prefix: either "s" in the case of fully stacked nucleobases or "ns" if they are nearly stacked. Accordingly, "s35" stacking of consecutive nucleotides corresponds to intrastrand stacking in an A-form helix.

In addition, we manually evaluated the conformations of the A-sites in a large set of redundant structures (http://rna.bgsu.edu/rna3dhub/nrlist; accessed October 15, 2013)[52] of small ribosomal subunits to detect the S-turn2 conformation. A list of PDB structures which were considered is shown in Table S3 (Supporting Information).

■ RESULTS AND DISCUSSION

Features of the S-turn2 RNA Backbone Configuration. In the crystal structures of the mitochondrial A-site taken for this study, we have identified a specific "S-turn" configuration of the RNA backbone,[55] which resembles the shape of the letter S (marked in purple in Figure 2b−d). As elaborated below, this conformation can be classified as type 2 S-turn (abbreviated as S-turn2).

The term S-turn was first explicitly introduced by Correll et al. for the S-shape of the backbone in the sarcin−ricin RNA motif[55] and later described by Duarte et al. as part of an S-motif.[56] However, this specific RNA backbone conformation was observed even earlier in loop E[57] and sarcin−ricin motifs.[58] Duarte et al. defined the full S-motif within the sarcin−ricin motif as a double-stranded segment composed of altogether seven nucleotides in two strands, and they introduced a new

class called the S2-motif, which has a slightly different backbone conformation in comparison to the S-motif.[56] This classification, however, may be confusing, because both S and S2 motifs were actually defined using the backbone conformation of solely one strand (i.e., the second strand is not needed for the definition). More recently, naming S-turn1 and S-turn2 on the basis of conformation of five and three consecutive nucleotides, respectively, was introduced by Wadley et al.[59] We adopt this nomenclature in the current work.

In this paper, we describe S-turn2 (Figure 3) using four nucleotides $N1-N4$ and the three backbone suites linking
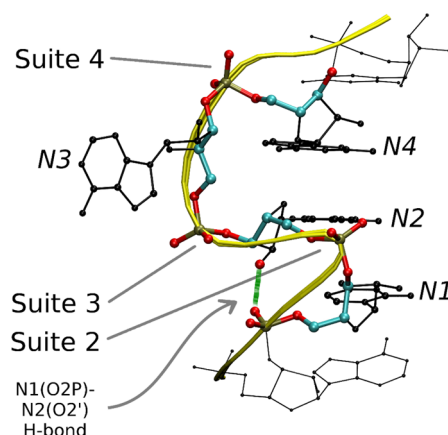

Figure 3. Conformation of S-turn2 in the human mitochondrial A-site variants. Gray arrow indicates the crucial H-bond interactions. The nucleotides $N1$, $N2$, $N3$, and $N4$ involved in the S-turn2 and backbone suites (as defined by Richardson et al.[54]) are labeled. The hydrogens are not shown for clarity.

them, according to the standard RNA backbone classification by Richardson et al.[54] (see Methods for details). Both types of S-turn reverse chain direction between $N1$ and $N2$, creating a sharp backbone bend. Backbone suite 2 (linking $N1$ and $N2$) is classified as **5z**[54] and stabilized by the O2P($N1$)−O2′($N2$) H-bond. The backbone progression is restored by backbone suites 3 and 4 between $N2$ and $N4$. Stacking interaction between $N1$ and $N2$ is classified as s33 and between $N2$ and $N4$ as s55 (cf. Sarver et al.[51]). The common feature of suites 3 and 4 in both types of S-turn is the C2′-endo pucker.[54] However, although the structure of S-turn1 is sharply defined (cf., e.g., the sarcin−ricin motif[55]), S-turn2 is more geometrically variable. In most cases, consecutive suites in S-turn2 can be described as $N01aN15zN26pN38dN41aN5$ (Ni is a ribonucleotide and the following two bold characters symbolize a family of a backbone suite associated with the $i + 1$ phosphate; nomenclature details are in the Methods section and in ref 54). However, we also observe a variation with $N32aN4$ (see S-turn2 occurrences listed in Table S4, Supporting Information). Finally, the most salient difference between the two S-turns is that S-turn2 has a flipped-out $N3$ nucleotide, whereas S-turn1 has $N3$ flipped-in into the major groove, to form a GpU dinucleotide platform (Figure 3).

Our bioinformatics analysis reveals that the characteristics of S-turn2 provided above matches well the RNA backbone conformations that appear in the crystallographic structures of the mitochondrial A-site constructs shown in Figure 2, with the flipped-in A1492 ($N2$ in Figure 3), flipped-out A1493 ($N3$), and all backbone suites matching the S-turn2 families.

Occurrences of S-turn2 in the Crystal Structures of the Ribosomes. We did not find any S-turn2 configuration in the crystal structures of the small ribosomal subunits and, in particular, in the A-sites of these structures (note that mitochondrial structure of the small subunit is not as yet available). However, we found S-turn2 occurrences in the large ribosomal subunit (Table 2), which are conserved, as shown in our sequence analyses. Their locations in the large subunit of *E. coli* are shown in Figure 4. Many occurrences of S-turn2 in structural data of the ribosome suggest that S-turn2 is functionally important.

Our analysis indicates that the S-turn2 formation does not require any specific sequence pattern (see data in Table 2). We observe that the flipped-out nucleotide ($N3$) is the most weakly conserved, and in general, the sequence conservations of the individual S-turn2 cases depend on their position in the ribosome. For instance, S-turn2 at the position 1944 (see Table 2) has a highly conserved sequence across all species, whereas the sequence conservation of S-turn2 at the position 801 across phylogenetic domains is weak. Also, there is no obvious sequence preference for any nucleotide forming S-turn2 (Ni in $N1-N4$), when grouping data for all their occurrences together (Table 2).

We found that the flipped-out S-turn2 nucleotides ($N3$ in Figure 3) in the conserved positions in the ribosome are involved in tertiary interactions with other parts of rRNA and are usually located in buried rRNA regions. This indicates that the S-turn2 occurrences in the large ribosomal subunit serve as static context-dependent structural elements connecting various fragments of rRNA; they form already during rRNA folding process and are remodeled by the context. On the other hand, we would expect S-turn2, that we found in the human mitochondrial A-site structures, to act as a dynamical molecular switch, which is necessary for proper functioning of A-site.[60] However, such functional duality of RNA structural features is not unusual. Another example of an RNA structural feature functioning in both dynamic and static modes is A-minor interaction type I. A-minor I interaction mostly serves as a stable tertiary interaction cementing the ribosome structure[61] but can act as a dynamical element facilitating functional motion.[62,63] A prominent example of the dynamical A-minor I interaction is actually the proofreading of the codon−anticodon double helix by the mRNA decoding center.

We also found S-turn2 instances in the bacterial ribosome that are located on the ribosomal surface: examples for *E. coli* are shown as green van der Waals spheres in Figure 4. The flipped-out nucleobase in these S-turn2 cases does not stack with other nucleotides and could be dynamic. However, these surface S-turns are located in rRNA regions which have nonconserved sequences, so their role (if any) in ribosome function is not clear.

Overall, our data indicate that the sequence conservation of a given S-turn2 is context-dependent. The context probably includes tertiary interactions as well as the flanking RNA sequences. However, basically any RNA sequence has propensity to adopt the S-turn2 topology within a suitable context. S-turn2 is probably intrinsically close in energy to canonical A-RNA single strand conformation, so that the RNA strand can be easily remodeled to adopt the S-turn2 topology. This is very different from the strict conservation of S-turn1.[64] The S-turn1 backbone topology is most likely intrinsically high in energy and thus can be adopted only by highly specific sequences (representing sarcin−ricin motif) with a dense

Table 2. Nucleobase Positions in the Large Ribosomal Subunits with Conserved S-turn2 Based on the Analysis of the Structural and Sequence Data Set

position of the bulged-out base in rRNA	kingdom	S-turn2 nucleotides				stacking		suites 2, 3, 4
		N1	N2	N3	N4	N1·N2	N2·N4	
801	archea	**G892**	C893	A894	A895	s33	s55	5z6p8d
	bacteria	**G799**	A800	G801	**A802**	s33	s55	5z6p8d
	eukaryota	*C931*	**U932**	*A933*	*G934*	s33	ns55	5z6p8d
1061	archea	**G1163**	**U1164**	G1165	A1166	s33		!! !! !!
	bacteria	**G1059**	**U1060**	*U1061*	**G1062**	s33		5z6p8d
	eukaryota	**G1234**	**U1235**	*G1236*	**G1237**	s33	ns55	5z !! !!
1699	archea	A1775	**A1776**	G1777	**A1778**	s33	s55	5z6p !!
	bacteria	G1697	**A1698**	G1699	**A1700**	s33	s55	5z6p !!
	eukaryota	*G1929*	**A1930**	U1931	**A1932**	s33	s55	5z6p2h
1816	archea	C1870	U1871	C1872	**G1873**	s33	s55	5z6p2a
	bacteria	**G1814**	**A1815**	C1816	**G1817**	s33	s55	5z !! 3a
	eukaryota	**U2173**	G2174	U2175	U2176	s33	s55	5z6p2a
1944	archea	**C1983**	**U1984**	*U1985*	**G1986**	s33	ns55	5z6p8d
	bacteria	**C1942**	**U1943**	**U1944**	**G1945**	s33		5z6p8d
	eukaryota	**C2285**	**U2286**	C2287	**G2288**	s33	ns55	5z6p !!
legend: sequence conservation		>98% (bold)		90—98% (italic)		80—90% (underlined)		

Search for S-turn2 conformation was performed on the nonredundant set of RNA structures including six large ribosomal subunit structures. Sequence conservation (in %) of each S-turn2 instance in the ribosome is based on Comparative RNA Web Site[7] rRNA alignments. The sequences and structural data (stacking, suites) are presented for the following representative structures: archea − PDB: 1S72, bacteria − 2QBG, and eukaryota − 3U5H. *E. coli* standard numbering of ribonucleotides is used. S-turn2 with the definition of nucleotides N1−N4 is shown in Figure 3. The nomenclature used in the last two columns (stacking and backbone suites) is described in the Methods section. Exclamation marks indicate unclassified backbone conformations.
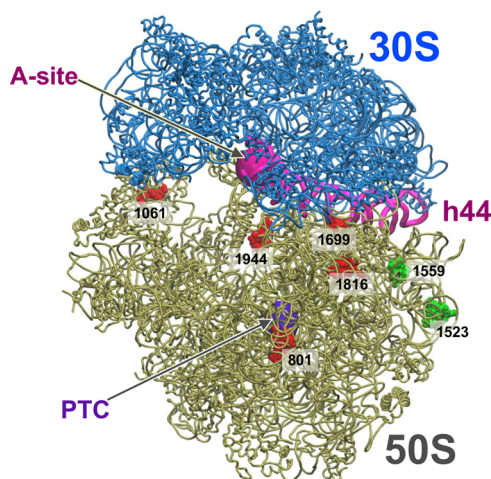

Figure 4. Positions of the S-turn2 motifs found in the large subunit of the *E. coli* ribosome. The conserved S-turn2 motifs represented by red van der Waals spheres are listed in Table 2; two nonconserved S-turn2 positions are marked in green (residue numbers of bulged-out nucleotides are shown). The 30S subunit is in blue, and 50S is in brown. Peptidyl transferase center PTC (violet sphere), A-site (magenta sphere), and h44 (in magenta) are marked for orientation. Figure is based on PDB files 2QBG and 2QBF.

network of stabilizing H-bonding and stacking interactions.[64] To the best of our knowledge, S-turn1 occurs only in the context of sarcin−ricin motifs. Thus, we suggest that despite some structural similarities, S-turn1 and S-turn2 backbone topologies are independent and unrelated RNA structural features with distinctly different physical−chemistry properties.

Why Is S-turn2 Formed in the Mitochondrial but Not in the Bacterial A-Site? Our search in the structures of the A-sites in the bacterial small ribosomal subunits (275 PDB files, Table S3) has shown no single instance of S-turn2. Also, there is no tendency to form S-turn2 in our MD simulations of the crystallographic model of the bacterial A-site, although the simulations obviously are not fully converged. In contrast, all three studied crystal models of human mitochondrial A-site contain the S-turn2 conformation at least in one site (Figure 2). Therefore, this observation raises an important question: why is S-turn2 found in mitochondrial variants but not in any bacterial A-site? The reasons may be as follows.

In the overall search, we identified altogether 46 instances of local (i.e., with N1−N4 nucleotides belonging to a continuous single RNA strand) S-turn2 (Table S4, Supporting Information). In these 46 instances, we did not find (by visual inspection) cases of internal loops with cWW base pairs flanking the looped-out N3 from both sides. This suggests a conflict between cWW base pairing of neighboring nucleotides and the S-turn2 backbone conformation. Virtually all ribosomal A-site internal loops have a universally conserved canonical G1494:C1407 base pair from one side, whereas there is sequence variability in the 1409:1491 and 1410:1490 pairs at the other side.[7] Our alignment of the bacterial A-site rRNA sequences reveals the following pattern (Table 3). Even if there are sequence differences in the 1409:1491 and 1410:1490 base pairs (for sequence numbering see Figure 1), these pairs are A:U or G:C, that is, most probably canonical cWW, in 98−99% of the bacterial species (the rest could be sequence misalignments). On the other hand, in the eukaryotic mitochondrial A-sites, there are many more sequence and potential base pairing

Table 3. Possible Base Pair Combinations and Their Occurrences (in %) at Positions 1409:1491 and 1410:1490 in Bacterial and Eukaryotic Mitochondrial A-Sites

bacterial			
1409:1491		1410:1490	
sequence	%	sequence	%
C:G	92.9	A:U	77.8
A:U	5.7	G:C	20.3
U:A	0.6	G:U	1.3
canonical	99.2	canonical	98.1
mitochondrial			
1409:1491		1410:1490	
sequence	%	sequence	%
C:U	37.1	C:A	34.2
C:C	35.8	C:G	32.7
C:A	13.3	U:G	11.3
C:G	7.8	A:U	8.7
G:U	3.3	U:A	6.2
A:U	1.4	G:U	4.3
		G:C	2.5
canonical	9.6	canonical	50.1

Base pairs were calculated on the basis of the alignments for bacterial and eukaryotic mitochondrial 16S rRNA sequences using data from the Comparative RNA Web Site.[7] For clarity, only base pairs present in over 0.5% of sequences are shown. For rRNA sequences, secondary structures, and nucleotide numbering, see Figure 1.

variations at these positions. The analysis of eukaryotic mitochondrial sequences (Table 3) shows a lot of variation in the region flanking the A-site internal loop: 1409:1491 yields only 9% of potentially canonical cWW base pairs, and 1410:1490 about 50%. Therefore, the canonical base pairing surrounding A1492 and A1493 at both sides of the internal loop may be one reason for the absence of an S-turn2 conformation in bacterial A-site structures. In contrast, non-Watson–Crick pairing may increase probability of S-turn2 formation in the mitochondrial ribosomes.

Furthermore, in our simulations of the human mitochondrial mutated systems with S-turn2, we observed frequent occurrence of a specific noncanonical base pairing combination: tHS of C1409:C1491 and tHH of A1408:A1492 (see Figure 5d,e). It lasted about 45–80% of time in the mitochondrial mutated variants (*MITO_MUT* and *MITO_MUT2*), but it was also populated to a certain extent in the *MITO* simulation, i.e. about 40–55% of time (see H-bond occupancies in Tables S5 and S6, Supporting Information). Because the nucleotide sequence in all mitochondrial variants (*MITO, MITO_MUT,* and *MITO_MUT2*) did not support the cWW base pairing but favored the tHS/tHH base pair pattern, we suggest that the noncanonical tHS(C1409:C1491)/tHH(A1408:A1492) combination is one of the native base pairing conformations of the mitochondrial A-site with S-turn2. Additionally, we note that in eukaryotic mitochondrial A-site sequences, approximately 85% of 1409:1491 base combinations (C:U, C:C, and A:C, see Table 3) would preferentially form a tHS base pair geometry, which is compatible with the S-turn1 in the framework of the sarcin–ricin motif.[65] Although we noted above that S-turn1 and S-turn2 are different backbone topologies, they share the same backbone suite in their bottom parts and may have similar sequence requirements for the bottom flanking base pairs.

These analyses suggest that the frequent observation of S-turn2 in crystallographic models of mitochondrial A-site is not incidental, and we may expect S-turn2 formation in the A-site of a human mitoribosome (and other eukaryotic mitochondrial ribosomes). It may result in a dynamical competition between conventional and S-turn2 backbone topologies in the mitochondrial A-site, which in addition could be highly tunable by details of the sequence.

Structural Stability of S-turn2 in MD Simulations. The fact that S-turn2 occurs in many different sequence and structure contexts (see Table 2 and Figure 4) implies that it is an easily accessible conformation which can be induced and stabilized by an appropriate context. This is in agreement with the simulations. Indeed, representative conformations derived from the clustering analyses shown in Figure S1 (Supporting Information) confirmed that S-turn2 motifs in our MD simulations of various A-sites were very structurally stable (i.e., observed for a significant fraction of time), and A1492/93 did not flip. For example, in the *MITO* and *MITO_MUT* variants, the cluster representatives presented in Figure S1b,c show that A1492 and A1493 did not distinctly change their initial backbone conformation and that A1493 nucleobase was locked in an extra-helical configuration in entire MD trajectories. This structural stability is also confirmed by low RMSD values from the starting structure for the backbones of nucleotides 1491−1494, which for *MITO/MITO_MUT* are in the range 0.8−1.0 (±0.1−0.2) Å depending on the site; for comparison, in a relatively immobile *S1* site of the *BACT* system, the corresponding RMSDs were equal to 1.1 ± 0.3 Å. Sub-microsecond simulations cannot be considered as converged and cannot resolve which conformational substate is more stable. However, structural stability in sub-microsecond simulations confirms that S-turn2 is a significant substate which can be involved in structural dynamics of the mitochondrial A-site.

To further test structural stability of S-turn2, we performed MD simulations of single RNA strands including this motif (Table 1). We observed unfolding of S-turn2 only in one simulation (for details see Section S1 in Supporting Information). In all other simulations, the S-turn2 was structurally stable and did not unfold despite lack of any support through interactions with the second strand. This means that the S-turn2 topology, once formed, is enveloped by sound intrinsic free energy barriers. Structural stability of the single strand simulations suggests that S-turn2 structure is, at least as a local energetic minimum, independent of the interactions with the opposite RNA strand.

Although the simulations are obviously not converged, they convincingly show that the S-turn2, once formed, would have reasonable lifetimes and would be structurally well-defined. It is thus well poised to be involved in functional dynamics of the A-site as one of the major players. The simulations reveal that the structurally stable backbone of S-turn2 shown in Figure 3 is unlikely to change its geometry without the breaking of base−base stacking and without a large scale rearrangement of neighboring nucleotides of the internal loop. The flipped-out nucleobase is thus locked in a specific extrahelical conformations and flipping back toward the minor groove is suppressed by a considerable energetic barrier. Although the accuracy of the classical force fields could be limited in describing the properties of such an atypical, complex RNA backbone conformation, the results seem to be qualitatively unambiguous.
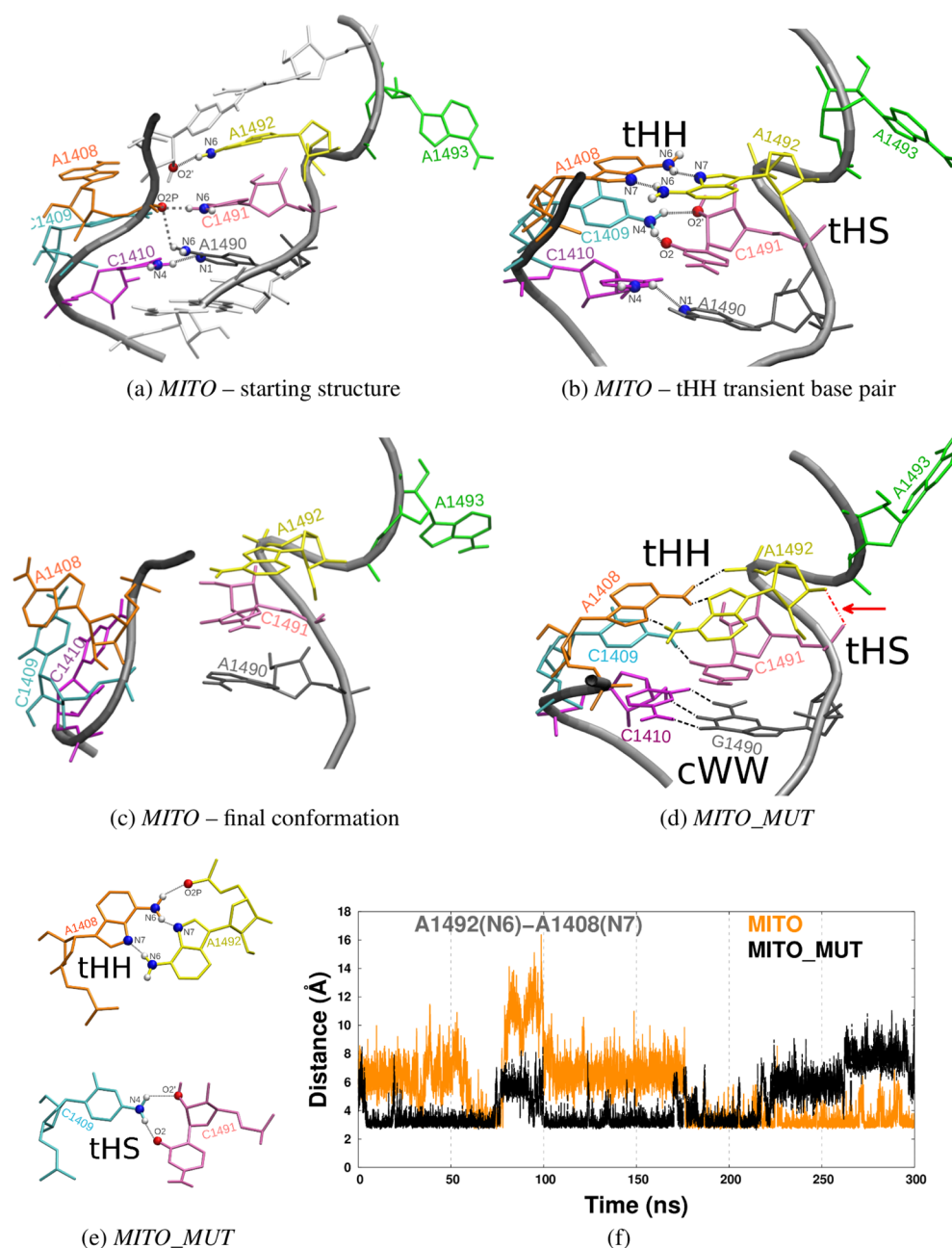
(a) *MITO* – starting structure

(b) *MITO* – tHH transient base pair

(c) *MITO* – final conformation

(d) *MITO_MUT*

(e) *MITO_MUT*

(f)

Figure 5. Typical MD conformations of the human mitochondrial A-site (wild-type and mutated) with S-turn2. (a)–(c) Various conformations of site *S1* of the mitochondrial A-site: (a) starting structure; (b) temporary formation of the tHH transient base pair; and (c) the final configuration of the A1408·C1409·C1410 stacked block. (d) Conformations of site *S1* of the human mitochondrial A-site A1490G mutant with S-turn2 (the O2'(A1492)−O2P(C1491) H-bond is indicated by red arrow). (e) Stable H-bonds for the two base pairs A1408:A1492 and C1409:C1491 in *S1* of the mutant. (f) Plot of the N6(A1492)−N7(A1408) H-bond distance in site *S1* of the *MITO* and *MITO_MUT* systems. For nucleotide sequences, see Figure 1. The non-polar hydrogens are not shown for clarity.

Overall Mobility of the Mitochondrial A-Site without S-turn2 Conformation Resembles Bacterial A-site. Interestingly, some X-ray structures of the mitochondrial A-site model lack the S-turn2 arrangement, e.g., site *S2* of the crystal structure 3BNS used for the *MITO_MUT2* simulation (Figure 1d). We found that the A1492/93 configuration and dynamics in this site resembles that of the bacterial A-site (compare conformations in Figure 6 for *BACT* and Figure 7 for *MITO_MUT2*). Also, the initial MD base pairing of A1408:A1493 in these sites was cWW (Figures 6a and 7a). Further, in MD simulations similar tHS schemes of A1408:A1493 were observed (Figures 6b and 7b). The

adenines 1492/93 in these MD trajectories remained in the intrahelical conformations. Furthermore, the MD-derived conformations of both A-site variants were similar to the conformations observed in our previous MD study[27] and in NMR experiments on bacterial A-site models (PDB codes 1PBR,[19] 1A3M[23]). Also, lack of S-turn2 in the mutated mitochondrial A-site rendered intrastrand nucleobase stacking in the A-site similar to that in the bacterial variant; in both cases A1408·C1407 stacking occurred over 70% of time, while in all the systems *with* S-turn2 stacking between A1408 and C1407 was not observed (Figure S2, Supporting Information).
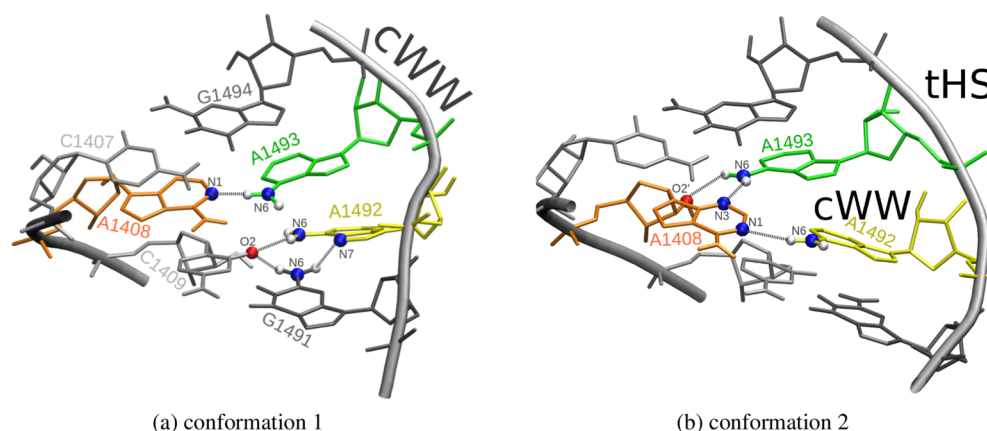
6694

dx.doi.org/10.1021/jp5030685 | *J. Phys. Chem. B* 2014, 118, 6687−6701

(a) conformation 1   (b) conformation 2

Figure 6. Hydrogen bonding patterns in MD simulations of the bacterial A-site. The exemplary conformations of the *BACT* variant (site *S1*): (a) cWW bifurcated A1493:A1408 base pair and C1409/G1491/A1492 triple; (b) tHS A1408:A1493 base pair and A1492 interacts with A1408 via Watson−Crick edges. For the nucleotide sequence, see Figure 1. The non-polar hydrogens are not shown for clarity.

Still, the MD behavior of the bacterial sites and its equivalent mitochondrial site arrangement differed in certain aspects. The latter variant of A-site displayed higher overall flexibility, as illustrated by the results of clustering in Figure S1a,d in Supporting Information. We observed reversible breaking of the canonical C1407:G1494 base pair (details not shown), which is present in almost all bacterial ribosomal crystal structures. Moreover, in the mitochondrial variant without S-turn2, the A-site nucleobases, including A1492/93, tended to move toward the major groove (Figure 7c), opposite to the expected motion in the ribosomal A-site during mRNA decoding.[60] Due to this conformational tendency in the mitochondrial system, it could be less probable for A1492/93 to acquire their "active" conformations (i.e., flipped-out in the direction of minor groove) in order to create a complex with (A-site)−tRNA.

In summary, dynamics of the two observed conformational states in the mitochondrial A-site: *without* S-turn2 (the "bacterial-like" state) and *with* S-turn2 are distinctly different. Also, we observed that in the simulations of double-stranded A-site models, these two states did not change from their starting conformations; S-turn2 did not unfold and did not spontaneously form. Therefore, the formation of S-turn2 seems to restrict backbone rearrangements, which may be the reason for lack of A1492/93 flipping in the sites with the S-turn2 backbone. In contrast, in the bacterial A-site, which does not acquire the S-turn2 conformation, we observed rapid flipping-in of A1492 in site *S2* from the initially extra-helical to intrahelical conformation (Figure 2a). Thus, it seems that the conformation of S-turn2 in mitochondrial A-sites precludes flipping and restricts the mobility of the A-site to a stable "inactive" conformational state (with A1492 flipped-in and A1493 flipped-out). This implies that, due to S-turn2 formation, the energetic barrier for A1492/93 flipping in the mitochondrial A-site might be higher than in the bacterial A-site.

Conformational Changes of A1408·C1409·C1410 Stacked Nucleobases in the Human Mitochondrial A-Site. In the native mitochondrial A-site, we noted increased mobility of nucleotides in the strand opposite to A1492/93. In *MITO*, the fluctuations of these nucleotides (Figure S3, Supporting Information) were distinctly higher than in all other variants. Clustering analysis (Figure S1b, Supporting Information) shows that the entire A1408·C1409·C1410 stacked block (further referred to as "*ACC*") was flexible,

especially in site *S1*. The conformations illustrating the collective movement of the *ACC* stack in site *S1* of *MITO*, inside and outside the A-site internal loop, are shown in Figure 5. In the starting structure, *ACC* was in an intrahelical conformation in both sites (Figure 5a). Further, A1408 and A1492 formed a semistable tHH base pair along with tHS C1409:C1491 base pair, as shown in Figure 5b. A full flipping-out of *ACC* (Figure 5c) occurred a few times in the trajectory in site *S1*, which is visualized by the distances between the H-bonding atoms of the opposite A1492 and A1408 in Figure 5f.

Interestingly, the fluctuations of the *ACC* nucleobase block (Figure S3) were distinctly lower in the sites of the A1490G mutated mitochondrial variants (*MITO_MUT* and *MITO_-MUT2*). For A-sites that adopt the S-turn2 conformation, tHH A1408:A1492 base pairing in the mutants was more stable than in the native variant (50−80% versus 40−55% of time, respectively, see Table S6 Supporting Information). Also, C1409 and C1491 formed a relatively stable tHS configuration (about 45 or 80% of time in *S1* or *S2* sites of *MITO_MUT* and about 75% in *S1* of *MITO_MUT2* simulation, see Table S5 Supporting Information). In contrast, this C1409:C1491 base pair, stable in the mitochondrial mutant, was just temporarily formed in the native variant, *MITO* (compare Figure 5b and 5d).

The observed high mobility of the *ACC* stack in the *MITO* system (and its lack in the mutants) may arise from the specific base pair geometry in this A-site variant. The A:C base combination rarely forms the cWW conformation,[66] and even if it does occur, it requires protonation of the adenine.[49] In the X-ray structure of the nonmutated mitochondrial A-site (Figure 2b), A1490 and C1410 interact by Watson−Crick edges in the *cis* conformation, but, when compared to canonical A:U, they are sheared in the opposite direction than the (protonated)−cWW A:C described by Leontis et al.[49] (see comparison of base pair geometries in Figure 8). Therefore, the crystal structure shows unprotonated cWW-like conformation of the base pair. The shear of cWW C1410:A1490 disfavors the tHS geometry of adjacent C1409:C1491, which is compatible with the canonical 1410:1490 combination. Finally, this prevents stable base pairing of the *ACC* nucleotides with the opposite RNA strand.

Furthermore, stacking interactions could explain why the *ACC* nucleobases tend to move collectively in *MITO* simulation. In all mitochondrial systems, A1408·C1409 and
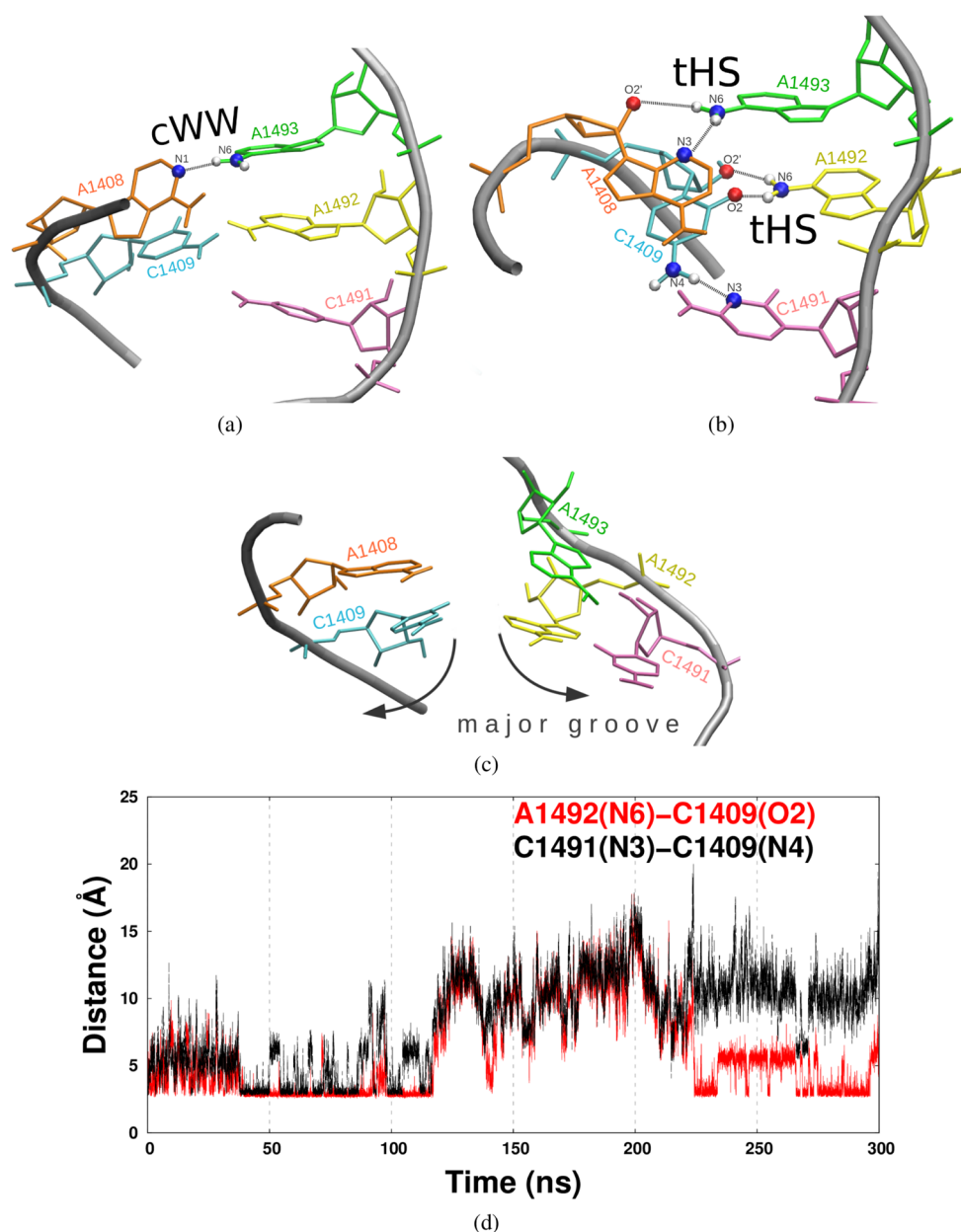
Figure 7. Typical MD conformations of the mitochondrial A-site A1490G mutant *without* S-turn2. (a) Starting conformation, (b) conformation showing semistable tHS base pairing of A1408:A1493 and C1409:A1492, and (c) showing the nucleobases shifted toward major groove. The conformations are representative of clusters derived from the *MITO_MUT2* simulation for site *S2*. (d) Distances for selected H-bonds shown in (b). For nucleotide sequence, see Figure 1. The non-polar hydrogens are not shown for clarity.

C1409·C1410 nucleobase stacking was at least as stable as in the *BACT* simulation (the percentage of time the nucleobases were stacked in each variant is shown in Figure S2, Supporting Information). In *MITO* simulations, despite high mobility of the *ACC* nucleobases, they were stably stacked for over 80% of the time. As a result, in the *MITO* variant, the two well-stacked cytosines C1409 and C1410, not involved in stable canonical base pairs, may have driven A1408 out of the helix due to the stable *ACC* stacking interactions. It seems that the native mitochondrial A-site variant specifically tunes the balance of intrastrand stacking and interstrand pairing in this region.

These observations indicate that the specific A1490:C1410 base pairing may induce larger fluctuations in the native mitochondrial A-site. Furthermore, the distinct stacking interactions within the *ACC* block may further promote its

concerted movement. The resulting *ACC* mobility in the nonmutated mitochondrial A-site, in particular, mobility of A1408, may affect aminoglycoside binding in the A-site, as discussed below.

Human Mitochondrial A-Site—Wild-Type versus A1490G Mutant and Consequences for Aminoglycoside Binding. In the sequences of the eukaryotic mitochondrial A-site, the 1410:1490 base pair is in about 30% of cases C:A and 30% of cases C:G (see sequences in Figure 1 and Table 3). Also, if we assume cWW base pairing, all the base combinations in Table 3 would be isosteric or nearly isosteric to the canonical C:G and U:A (classification by Stombaugh et al.[66]). This implies that all these sequence variations, including human A1490G mutation, should be neutral for proper functioning of mitoribosomes.
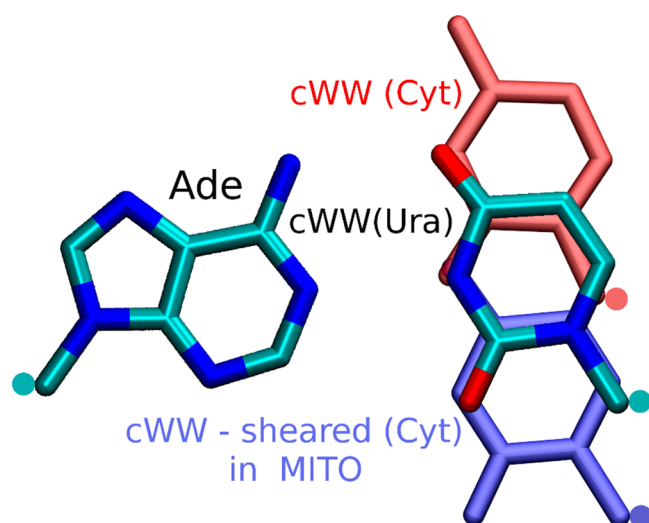
Figure 8. Conformations of cWW A1490:C1410 base pair in the human mitochondrial A-site. Canonical cWW A:U base pair is colored by atom type; the cWW A:C geometry according to Leontis et al.[49] is colored red, and the cWW A:C sheared base pair, observed in X-ray structures, is colored blue. The positions of the C1′ atoms are represented by red, blue, and cyan dots. Note that the cWW A:C base pair (in red) is protonated following Leontis et al.,[49] whereas the A-site base pair is not protonated. The hydrogens are not shown for clarity.

However, the C:A cWW base pair is not as stable as the canonical pairs and this may explain flexibility and alternative substates of the decoding site in the *MITO* variant. In the human mitochondrial A1490G mutant, the formation of a stable canonical C1410:G1490 base pair (instead of C:A, Figure 1) makes the secondary structure of the mutant resemble the bacterial A-site, which is the primary target of aminoglycosides. Moreover, during the MD simulations, the more stable C1410:G1490 base pair locked the A1408·C1409·C1410 block in a flipped-in position. These dynamical differences between native and A1490G mutated mitochondrial systems might explain their different susceptibility to aminoglycosides. Experiments performed on hybrid ribosomes containing the human mitochondrial A-site—native or A1490G mutated sequence—showed that minimal inhibitory concentrations of aminoglycoside required to inhibit bacterial growth (MIC) are higher for the native variants. For example, MIC values for tobramycin were 128 μg/mL for the native mitochondrial variant and 16 μg/mL for the mutant, and MIC values for paromomycin were >1024 for the nonmutated and 256−512 μg/mL for the mutant.[10] This behavior is expected because different dynamics of the A-site variants, arising from the mutation, may contribute to these different antibiotic activities.

Moreover, experiments suggested that, apart from the general electrostatic-driven complexation, the size and shape of aminoglycoside RNA targets are important factors determining the antibiotic binding.[67] The shape and flexibility of the RNA target seem to be more important for aminoglycoside binding than their specific interactions with a specific nucleobase. Therefore, the observed flipping of the *ACC* nucleobases in the *MITO* trajectories may simply overly increase the volume of the aminoglycoside binding site in the mitochondrial A-site. Flipping-out of the stacked 1409·1410 nucleobases is sterically constrained only to a certain extent within the context of the complete ribosome. The mobility of A1408 may be hindered only by the interactions with the H69 helix from the 50S

subunit, but it is not entirely blocked, as illustrated in Figure 9a,c in the crystal structure of the bacterial ribosome (note that the human mitochondrial ribosome structure is not available).
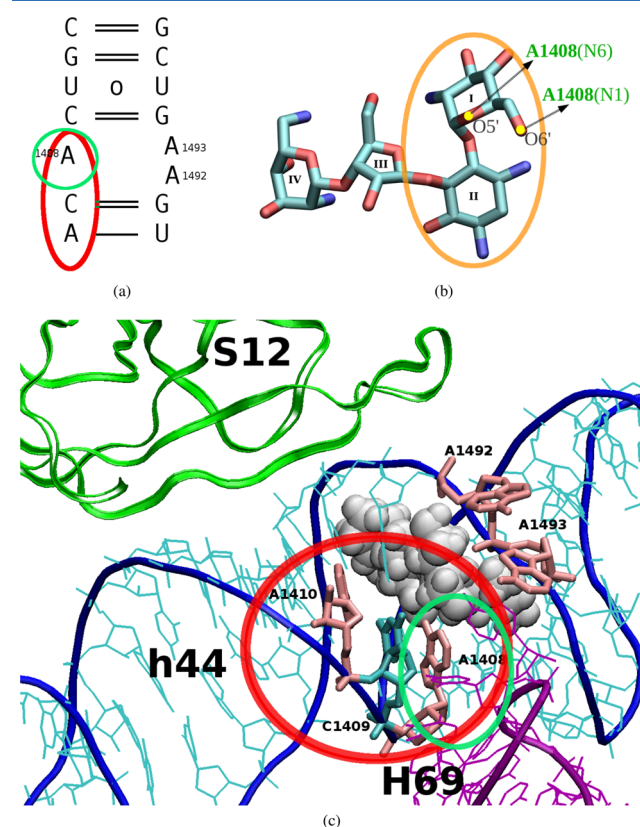

Figure 9. Location of the A1408·C1409·A1410 (*ACA*) nucleobases in the bacterial ribosome. (a) Secondary structure of the bacterial A-site with the crucial A1408 in green circle and the *ACA* nucleotides in red ellipse; (b) paromomycin with the two oxygen atoms of the neamine core (encircled orange) H-bonding with A1408 of the A-site; (c) the *ACA* segment in the context of the full bacterial ribosome with an aminoglycoside paromomycin shown as white spheres. The hydrogens are not shown for clarity.

Based on the above observations, one possible explanation of the higher activity of aminoglycosides against the mutated mitochondrial A-site could be the stochastic gating mechanism, postulated by Vaiana et al.,[4] for aminoglycoside binding in the A-site. Because the position of the ACC block in the *MITO* simulations fluctuates considerably, the population of the binding sites with the shape favorable for aminoglycoside binding is lower than in the mutant, leading to less states allowing for aminoglycoside binding. On the other hand, the mobility of the *ACC* stack could also affect some crucial interactions of aminoglycoside with its target. In the full bacterial ribosome, the "neamine core" of aminoglycoside antibiotics forms stable H-bonds with A1408[29] (see Figure 9b). The movement of the stacked *ACC* nucleobases out of the helix could disrupt the crucial H-bonds that A1408 has to form with an aminoglycoside. This could change the binding mode and lead to different inhibition efficiencies of these antibiotics against the mutated human mitochondrial A-site versus the wild-type equivalent.

Note that the structural effects in different variants of mitochondrial A-site discussed above do not need to be exclusive. For affecting the aminoglycoside binding affinities it
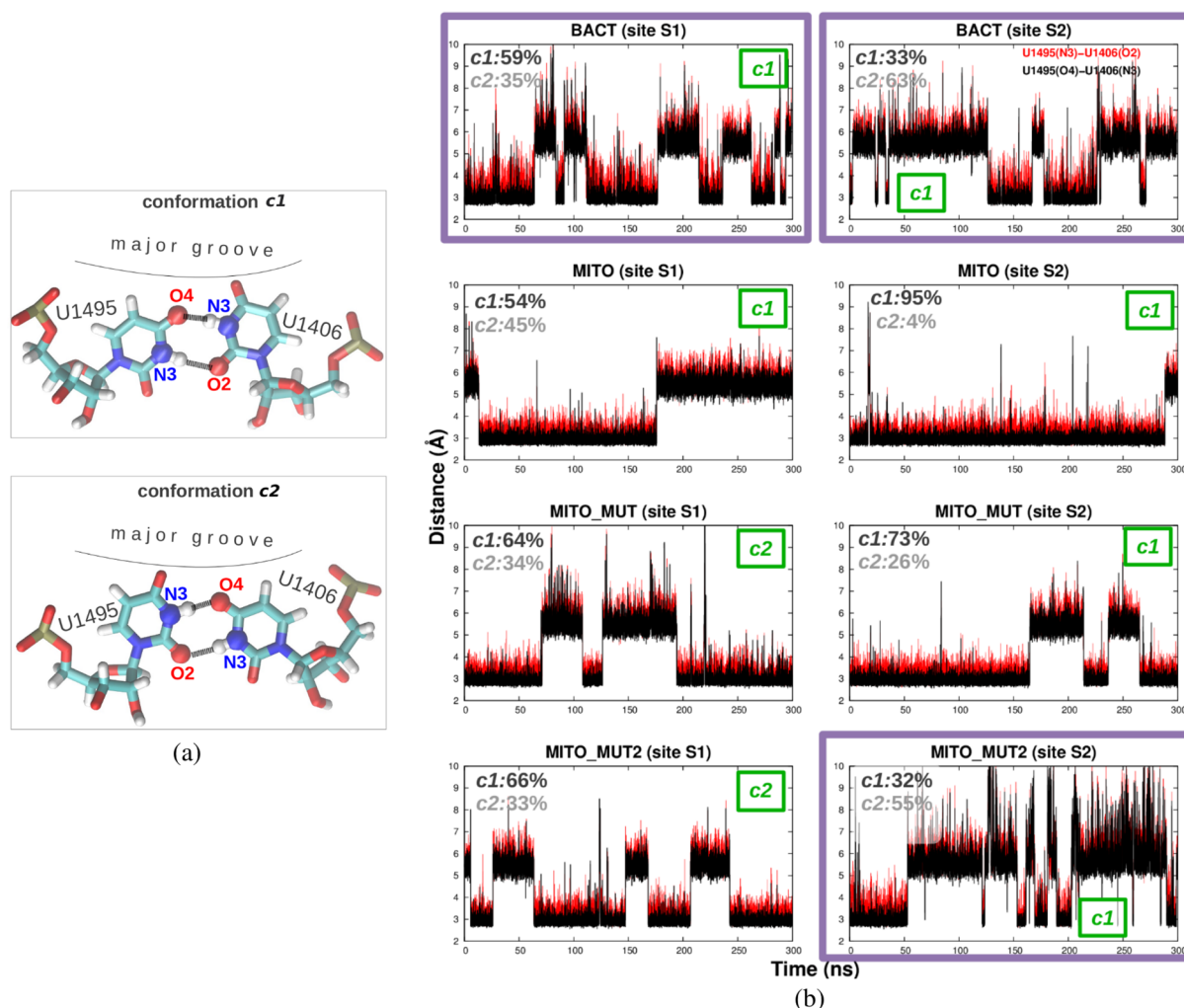
Figure 10. Mobility of uracils 1406 and 1495 over MD simulation time. (a) The two typically observed base pairings of U1406:U1495 ($c1$ and $c2$); (b) the H-bond distances corresponding to the $c1$ conformation versus simulation time for different A-site variants and sites. Plots for the sites *without* S-turn2 conformation are in violet frames. The MD-derived occupancies (in %) of conformations $c1$ and $c2$ are shown for each variant. The U:U conformations of the starting crystal structures are denoted in green boxes. The crystallographic structures used in MD simulations, with the definition of sites, are shown in Figure 2.

would be entirely sufficient to change populations of the different substates and thus the balance of free energies. As an additional contribution, the change in the aminoglycoside binding mode might reduce antibiotic activity in promoting "active" states of A1492/93 in the decoding center.

Conformation of U1406:U1495 Base Pair Differs in Bacterial and Human Mitochondrial A-Site. The U1406:U1495 cWW base pair, located near the A-site internal loop in proximity to A1492 and A1493 (see Figure 1), has been found crucial for the structure and function of the ribosomal A-site.[8,27,29,68] Computational studies also suggested that this U:U pair is important for aminoglycoside positioning in the A-site.[27,29] U:U can adopt two distinct conformations, denoted here as $c1$ and $c2$; both are observed in the ribosomal A-site models, including the starting crystal structures used in this study[9] (see Figure 10a). However, in complete bacterial ribosome structures, these uracils almost exclusively adopt the $c2$ geometry. In MD simulations of the bacterial A-site model in the complex with paromomycin, Vaiana et al.[29] observed that the binding mode of the antibiotic slightly differs depending on the U:U conformation ($c1$ or $c2$). They proposed that the $c1$ conformation is a consequence of the small inaccuracy of the

starting crystal structure. However, we observed the $c1$ configuration of U:U in all our MD simulations.

In all A-site variants, the U1406:U1495 conformations interconverted (Figure 10b). In the *BACT* system the dominant conformation depended on the site: in the less mobile *S1*, it was mostly $c1$, and in *S2*, it was mostly $c2$ (for the definition of sites see Figure 1 and 2). In all human mitochondrial variants *with* S-turn2, the $c1$ configuration was dominant (even in the sites with the $c2$ configuration in the starting structure, i.e., site *S1* in *MITO_MUT* and *MITO_MUT2*). In contrast, $c2$ was dominantly populated in the mitochondrial site *lacking* S-turn2 (i.e., site *S2* in the *MITO_MUT2* system). Therefore, the $c1$ U:U geometry seems to be more compatible with the S-turn2 backbone configuration. Moreover, as shown in Figure 10b, during 300 ns trajectories, in sites of the mitochondrial variants *with* S-turn2, there were only two to six exchanges between the two conformations $c1$ and $c2$. In the systems *without* S-turn2 (i.e., *BACT* and the *S2* site of *MITO_MUT2*), we observed about 10 $c1/c2$ conformational exchanges. This suggests that the S-turn2 also hinders the conformational changes of the neighboring pair of uracils.

Because we observed both conformations of the U:U pair in each simulated A-site variant, we suggest that in small A-site RNA models, this base pair exists in a dynamic equilibrium between these two geometries. On the other hand, the U:U behavior in the full ribosome is constrained by the ribosomal surrounding, and these interactions may enforce the *c2* conformation observed in the crystal structures of complete bacterial ribosomes. These constraints may alter the A-site dynamics in the full ribosome versus the small oligoribonucleotide model, as found in our other MD study (data not shown).

◼ CONCLUSIONS

We performed MD simulations of the bacterial and human mitochondrial ribosomal A-site variants (native and A1490G mutant) with an aggregate time of about 6.1 μs and compared their structural dynamics. We have also carried out structural and sequence bioinformatics analysis of RNA S-turn2 motif in available RNA crystal structures and compared it with S-turn1 motif that occurs in the sarcin–ricin loop.

In the X-ray structures of the isolated mitochondrial A-site, we characterized a specific RNA backbone topology, S-turn2, which was not observed in any crystal structure of the bacterial A-site. We detected S-turn2 occurrences in the crystallographic data of ribosome structures of species in different phylogenetic domains, but only in the large subunits. We did not find S-turn2 in any available crystal structure of the small subunit, including their A-sites. We found no global S-turn2 sequence conservation, but distinct sequence conservation patterns can be found for some specific S-turn2 occurrences. We conclude that the formation of S-turn2 conformation may be adopted by a wide range of RNA sequences, and its actual formation is related to (induced by) specific RNA structural contexts.

Regarding the A-sites, we suggest that the absence of S-turn2 in the experimental structures of bacterial A-sites arises from canonical base pairing, and the presence of S-turn2 in the mitochondrial A-sites arises from a specific noncanonical base pairing. We propose that the nucleobases flanking the internal loop of the mitochondrial A-site have propensity for non-canonical pairing, which is more compatible with the S-turn2 configuration than the canonical pairing in the bacterial variant. Our MD simulations also indicated that the formation of S-turn2 may hinder the U1406:U1495 noncanonical base pair conformational exchanges. We observed that one of the U:U conformations (*c1*) occurs more frequently in sites including S-turn2, which suggests that S-turn2 may favor this particular conformation of uracils in the A-site.

MD simulations show that the S-turn2 backbone configuration is stable, even if simulated as a single strand. We did not observe changes in the conformation of the S-turn2-forming RNA backbone from the initial structure. The observed S-turn2 structural stability suggests that this motif may be a significant long-living substate, involved in the dynamics of the human mitochondrial A-site but not in the dynamics of the bacterial A-sites. We also found that the dynamics of human mitochondrial A-site with and without S-turn2 differs and specifically modulates the conformational behavior of A1492 and A1493. The dynamics of the human mitochondrial A1490G variant without the S-turn2 resembles that of the bacterial A-site and shows preference for intrahelical states of A1492 and A1493. These observations are consistent with the hypothesis by Kondo et al.,[9] suggesting that the two distinctly different configurations observed in crystal structures of mitochondrial A-site (*with* and *without*, herein described, S-turn2) may be

functionally important for mRNA decoding, and may be separated by an even higher energetic barrier than the flipped-in and flipped-out states of A1492 and A1493 in bacteria. This would lead to a "harder" molecular switch in mitochondria between the active and inactive A-site conformations and could cause higher accuracy of mRNA decoding in mitochondria than in bacteria. Further, this is consistent with lower number of tRNAs in mitochondria than in the cytoplasm and a lower number of proteins that need to be synthesized in mitochondria.[69]

We also identified a possible reason for the stronger binding of aminoglycosides toward the human mitochondrial A1490G A-site mutant than to the native mitochondrial A-site. In the latter, we observed collective movement of a stacked nucleotide A1408·C1409·C1410 block (*ACC*), which resulted from geometrical incompatibility of the consecutive C1410:A1490 and C1409:C1491 base pairs. The mobility of this *ACC* block could disrupt or weaken the stable H-bonds which A1408 forms with aminoglycoside antibiotics bound in the A-site. Therefore, the movement of the *ACC* block in the native mitochondrial A-site may be the reason for destabilization of binding of the neamine core of aminoglycosides. Also, its movement increases the volume of the RNA internal loop, which was shown to be related to aminoglycoside binding.[67] Overall, we described the conformational differences between the bacterial and mitochondrial A-sites that may affect the speed and accuracy of mRNA decoding and binding affinities of aminoglycoside antibiotics.

◼ ASSOCIATED CONTENT

⑤ Supporting Information

Supporting Information consists of a single PDF document containing Section S1, Tables S1–S6, and Figures S1–S5. Section S1 describes unfolding of S-turn2 observed in one MD simulation, and the corresponding structural details are illustrated with Figure S5 and S6. Table S1 characterizes in detail crystal structures taken for MD study. Tables S2–S4 present details of the bioinformatic analysis of S-turn2. Tables S5 and S6 list H-bonds (and their occupancies) that were observed in MD simulations of RNA models containing the double A-site (see Table 1). Figures S1–S3 illustrate results of MD simulations for different variants of double A-site RNA models: (i) Figure S1 shows superposed cluster representatives of A-sites, (ii) Figure S2 shows stacking occupancies for nucleotides 1407–1410, and (iii) Figure S3 presents fluctuations of the nucleotides. This material is available free of charge via the Internet at http://pubs.acs.org.

◼ AUTHOR INFORMATION

Corresponding Authors
*E-mail: sponer@ncbr.muni.cz.
*E-mail: joanna@cent.uw.edu.pl.

Notes
The authors declare no competing financial interest.

■ REFERENCES

(1) Wimberly, B. T.; Brodersen, D. E.; Clemons, W., Jr; Morgan-Warren, R. J.; Carter, A. P.; Vonrhein, C.; Hartsch, T.; Ramakrishnan, V. Structure of the 30S Ribosomal Subunit. *Nature* **2000**, *407*, 327−339.

(2) Ogle, J. M.; Brodersen, D. E.; Clemons, W. M.; Tarry, M. J.; Carter, A. P.; Ramakrishnan, V. Recognition of Cognate Transfer RNA by the 30S Ribosomal Subunit. *Science* **2001**, *292*, 897−902.

(3) Sanbonmatsu, K. Y. Energy Landscape of the Ribosomal Decoding Center. *Biochimie* **2006**, *88*, 1053−1059.

(4) Vaiana, A. C.; Sanbonmatsu, K. Y. Stochastic Gating and Drug−Ribosome Interactions. *J. Mol. Biol.* **2009**, *386*, 648−661.

(5) Zhang, W.; Dunkle, J. A.; Cate, J. H. D. Structures of the Ribosome in Intermediate States of Ratcheting. *Science* **2009**, *325*, 1014−1017.

(6) Sanbonmatsu, K. Y.; Joseph, S. Understanding Discrimination by the Ribosome: Stability Testing and Groove Measurement of Codon−Anticodon Pairs. *J. Mol. Biol.* **2003**, *328*, 33−47.

(7) Cannone, J. J.; Subramanian, S.; Schnare, M. N.; Collett, J. R.; D'Souza, L. M.; Du, Y.; Feng, B.; Lin, N.; Madabusi, L. V.; Muller, K. M.; et al. The Comparative RNA Web (CRW) Site: An Online Database of Comparative Sequence and Structure Information for Ribosomal, Intron,and Other RNAs. *BMC Bioinformatics* **2002**, *3*, 2.

(8) Romanowska, J.; McCammon, J. A.; Trylska, J. Understanding the Origins of Bacterial Resistance to Aminoglycosides Through Molecular Dynamics Mutational Study of the Ribosomal A-Site. *PLoS Comput. Biol.* **2011**, *7*, e1002099.

(9) Kondo, J.; Westhof, E. The Bacterial and Mitochondrial Ribosomal A-Site Molecular Switches Possess Different Conformational Substates. *Nucleic Acids Res.* **2008**, *36*, 2654−2666.

(10) Hobbie, S. N.; Akshay, S.; Kalapala, S. K.; Bruell, C. M.; Shcherbakov, D.; Bottger, E. C. Genetic Analysis of Interactions with Eukaryotic rRNA Identify the Mitoribosome As Target in Aminoglycoside Ototoxicity. *Proc. Natl. Acad. Sci. U.S.A.* **2008**, *105*, 20888−20893.

(11) Kaul, M.; Barbieri, C. M.; Pilch, D. S. Defining the Basis for the Specificity of Aminoglycoside-rRNA Recognition: A Comparative Study of Drug Binding to the A Sites of *Escherichia coli* and Human rRNA. *J. Mol. Biol.* **2005**, *346*, 119−134.

(12) Kondo, J.; Hainrichson, M.; Nudelman, I.; Shallom-Shezifi, D.; Barbieri, C. M.; Pilch, D. S.; Westhof, E.; Baasov, T. Differential Selectivity of Natural and Synthetic Aminoglycosides Towards the Eukaryotic and Prokaryotic Decoding A Sites. *ChemBioChem* **2007**, *8*, 1700−1709.

(13) Yang, G.; Trylska, J.; Tor, Y.; McCammon, J. A. Binding of Aminoglycosidic Antibiotics to the Oligonucleotide A-Site Model and 30S Ribosomal Subunit: Poisson−Boltzmann Model, Thermal Denaturation, and Fluorescence Studies. *J. Med. Chem.* **2006**, *49*, 5478−5490.

(14) Francois, B.; Russell, R. J. M.; Murray, J. B.; Aboul-ela, F.; Masquida, B.; Vicens, Q.; Westhof, E. Crystal Structures of Complexes Between Aminoglycosides and Decoding A Site Oligonucleotides: Role of the Number of Rings and Positive Charges in the Specific Binding Leading to Miscoding. *Nucleic Acids Res.* **2005**, *33*, 5677−5690.

(15) Vicens, Q.; Westhof, E. Crystal Structure of Paromomycin Docked Into the Eubacterial Ribosomal Decoding A Site. *Structure* **2001**, *9*, 647−658.

(16) Cashman, D. J.; Rife, J. P.; Kellogg, G. E. Which Aminoglycoside Ring Is Most Important for Binding? A Hydropathic Analysis of Gentamicin, Paromomycin, and Analogues. *Bioorg. Med. Chem. Lett.* **2001**, *11*, 119−122.

(17) Kaul, M.; Barbieri, C. M.; Pilch, D. S. Fluorescence-Based Approach for Detecting and Characterizing Antibiotic-Induced Conformational Changes in Ribosomal RNA: Comparing Aminoglycoside Binding to Prokaryotic and Eukaryotic Ribosomal RNA Sequences. *J. Am. Chem. Soc.* **2004**, *126*, 3447−3453.

(18) Kaul, M.; Barbieri, C. M.; Pilch, D. S. Aminoglycoside-Induced Reduction in Nucleotide Mobility at the Ribosomal RNA A-Site as a Potentially Key Determinant of Antibacterial Activity. *J. Am. Chem. Soc.* **2006**, *128*, 1261−1271.

(19) Fourmy, D.; Recht, M. I.; Blanchard, S. C.; Puglisi, J. D. Structure of the A Site of *Escherichia coli* 16S Ribosomal RNA Complexed with an Aminoglycoside Antibiotic. *Science* **1996**, *274*, 1367−1371.

(20) Hobbie, S. N.; Kalapala, S. K.; Akshay, S.; Bruell, C.; Schmidt, S.; Dabow, S.; Vasella, A.; Sander, P.; Bottger, E. C. Engineering the rRNA Decoding Site of Eukaryotic Cytosolic Ribosomes in Bacteria. *Nucleic Acids Res.* **2007**, *35*, 6086−6093.

(21) Guthrie, O. W. Aminoglycoside Induced Ototoxicity. *Toxicology* **2008**, *249*, 91−96.

(22) Guan, M.-X. Mitochondrial 12S rRNA Mutations Associated with Aminoglycoside Ototoxicity. *Mitochondrion* **2011**, *11*, 237−245.

(23) Lynch, S. R.; Puglisi, J. D. Structure of a Eukaryotic Decoding Region A-Site RNA. *J. Mol. Biol.* **2001**, *306*, 1023−1035.

(24) Yoshizawa, S.; Fourmy, D.; Puglisi, J. D. Structural Origins of Gentamicin Antibiotic Action. *EMBO J.* **1998**, *17*, 6437−6448.

(25) Shandrick, S.; Zhao, Q.; Han, Q.; Ayida, B. K.; Takahashi, M.; Winters, G. C.; Simonsen, K. B.; Vourloumis, D.; Hermann, T. Monitoring Molecular Recognition of the Ribosomal Decoding Site. *Angew. Chem., Int. Ed.* **2004**, *43*, 3177−3182.

(26) Barbieri, C. M.; Kaul, M.; Pilch, D. S. Use of 2-Aminopurine as a Fluorescent Tool for Characterizing Antibiotic Recognition of the Bacterial rRNA A-Site. *Tetrahedron* **2007**, *63*, No. 10.1016/j.tet.2006.08.107.

(27) Romanowska, J.; Setny, P.; Trylska, J. Molecular Dynamics Study of the Ribosomal A-Site. *J. Phys. Chem. B* **2008**, *112*, 15227−15243.

(28) Reblova, K.; Lankas, F.; Razga, F.; Krasovska, M. V.; Koca, J.; Sponer, J. Structure, Dynamics, and Elasticity of Free 16s rRNA Helix 44 Studied by Molecular Dynamics Simulations. *Biopolymers* **2006**, *82*, 504−520.

(29) Vaiana, A. C.; Westhof, E.; Auffinger, P. A Molecular Dynamics Simulation Study of an Aminoglycoside/A-Site RNA Complex: Conformational and Hydration Patterns. *Biochimie* **2006**, *88*, 1061−1073.

(30) Dudek, M.; Romanowska, J.; Wituła, T.; Trylska, J. Interactions of amikacin with the RNA model of the ribosomal A-site: computational, spectroscopic and calorimetric studies. *Biochimie* **2014**, DOI: 10.1016/j.biochi.2014.03.009.

(31) Barbault, F.; Ren, B.; Rebehmed, J.; Teixeira, C.; Luo, Y.; Smila-Castro, O.; Maurel, F.; Fan, B.; Zhang, L.; Zhang, L. Flexible Computational Docking Studies of New Aminoglycosides Targeting RNA 16S Bacterial Ribosome Site. *Eur. J. Med. Chem.* **2008**, *43*, 1648−1656.

(32) Setny, P.; Trylska, J. Search for Novel Aminoglycosides by Combining Fragment-Based Virtual Screening and 3D-QSAR Scoring. *J. Chem. Inf. Model.* **2009**, *49*, 390−400.

(33) Carter, A. P.; Clemons, W. M.; Brodersen, D. E.; Morgan-Warren, R. J.; Wimberly, B. T.; Ramakrishnan, V. Functional Insights From the Structure of the 30S Ribosomal Subunit and Its Interactions with Antibiotics. *Nature* **2000**, *407*, 340−348.

(34) Case, D.; Cheatham, T.; Darden, T.; Gohlke, H.; Luo, R.; Merz, K. M., Jr.; Onufriev, A.; Simmerling, C.; Wang, C.; R, W. The Amber Biomolecular Simulation Programs. *J. Comput. Chem.* **2005**, *26*, 1668−1688.

(35) Case, D. A.; Darden, T. A.; Cheatham, T. E., III; Simmerling, C. L.; Wang, J.; Duke, R. E.; Luo, R.; Crowley, M.; Walker, R. C.; Zhang, W. et al. *AMBER 10*. University of California: San Francisco, 2008; http://ambermd.org/.

(36) Zhang, Z.; Sanbonmatsu, K. Y.; Voth, G. A. Key Intermolecular Interactions in the *E. coli* 70S Ribosome Revealed by Coarse-Grained Analysis. *J. Am. Chem. Soc.* **2011**, *133*, 16828−16838.

(37) Drsata, T.; Perez, A.; Orozco, M.; Morozov, A. V.; Sponer, J.; Lankas, F. Structure, Stiffness and Substates of the Dickerson−Drew Dodecamer. *J. Chem. Theory Comput.* **2013**, *9*, 707−721.

(38) Darden, T.; Perera, L.; Li, L.; Pedersen, L. New Tricks for Modelers From the Crystallography Toolkit: The Particle Mesh Ewald Algorithm and Its Use in Nucleic Acid Simulations. *Structure* **1999**, *7*, R55−R60.

(39) Ryckaert, J.; Ciccotti, G.; Berendsen, H. Numerical Integration of the Cartesian Equations of Motion of a System with Constraints: Molecular Dynamics of N-Alkanes. *J. Comput. Phys.* **1977**, *23*, 327−341.

(40) Reblova, K.; Fadrna, E.; Sarzynska, J.; Kulinski, T.; Kulhanek, P.; Ennifar, E.; Koca, J.; Sponer, J. Conformations of Flanking Bases in HIV-1 RNA DIS Kissing Complexes Studied by Molecular Dynamics. *Biophys. J.* **2007**, *93*, 3932−3949.

(41) Reblova, K.; Strelcova, Z.; Kulhanek, P.; Besseova, I.; Mathews, D. H.; Nostrand, K. V.; Yildirim, I.; Turner, D. H.; Sponer, J. An RNA Molecular Switch: Intrinsic Flexibility of 23S rRNA Helices 40 and 68 5′-UAA/5′-GAN Internal Loops Studied by Molecular Dynamics Methods. *J. Chem. Theory Comput.* **2010**, *2010*, 910−929.

(42) Cornell, W. D.; Cieplak, P.; Bayly, C. I.; Gould, I. R.; Merz, J.; M, K.; Ferguson, D. M.; Spellmeyer, D.; Fox, T.; Caldwell, J.; et al. A Second Generation Force Field for the Simulation of Proteins, Nucleic Acids, and Organic Molecules. *J. Am. Chem. Soc.* **1995**, *117*, 5179−5197.

(43) Perez, A.; Marchan, I.; Svozil, D.; Sponer, J.; Cheatham, T. E.; Laughton, C. A.; Orozco, M. Refinement of the AMBER Force Field for Nucleic Acids: Improving the Description of Alpha/Gamma Conformers. *Biophys. J.* **2007**, *92*, 3817−3829.

(44) Zgarbova, M. M.; Otyepka, M.; Sponer, J.; Mladek, A.; Banas, P. P.; Cheatham, T. E., III; Jurecka, P. Refinement of the Cornell Et Al. Nucleic Acids Force Field Based on Reference Quantum Chemical Calculations of Glycosidic Torsion Profiles. *J. Chem. Theory Comput.* **2011**, *7*, 2886−2902.

(45) Banas, P.; Hollas, D.; Zgarbova, M.; Jurecka, P.; Orozco, M.; Cheatham, T. E.; Sponer, J. S.; Otyepka, M. Performance of Molecular Mechanics Force Fields for RNA Simulations: Stability of UUCG and GNRA Hairpins. *J. Chem. Theory Comput.* **2010**, *6*, 3836−3849.

(46) Sponer, J.; Cang, X.; Cheatham, T. E., III Molecular Dynamics Simulations of G-DNA and Perspectives On the Simulation of Nucleic Acid Structures. *Methods* **2012**, *57*, 25−39.

(47) Dang, L. X.; Kollman, P. A. Free Energy of Association of the K+:18-Crown-6 Complex in Water: A New Molecular Dynamics Study. *J. Phys. Chem.* **1995**, *99*, 55−58.

(48) Berendsen, H. J. C.; Grigera, J. R.; Straatsma, T. P. The Missing Term in Effective Pair Potentials. *J. Phys. Chem.* **1987**, *91*, 6269−6271.

(49) Leontis, N. B.; Stombaugh, J.; Westhof, E. The Non-Watson-Crick Base Pairs and Their Associated Isostericity Matrices. *Nucleic Acids Res.* **2002**, *30*, 3497−3531.

(50) Petrov, A. I.; Zirbel, C. L.; Leontis, N. B. WebFR3D−A Server for Finding, Aligning and Analyzing Recurrent RNA 3D Motifs. *Nucleic Acids Res.* **2011**, *39*, W50−W55.

(51) Sarver, M.; Zirbel, C. L.; Stombaugh, J.; Mokdad, A.; Leontis, N. B. FR3D: Finding Local and Composite Recurrent Structural Motifs in RNA 3D Structures. *J. Math. Biol.* **2008**, *56*, 215−252.

(52) *RNA 3D Structure Analysis, Prediction*; Leontis, N., Westhof, E., Eds.; Nucleic Acids and Molecular Biology Series; Springer: Berlin, Heidelberg, 2012; Vol. 27.

(53) Davis, I. W.; Leaver-Fay, A.; Chen, V. B.; Block, J. N.; Kapral, G. J.; Wang, X.; Murray, L. W.; Arendall, W. B., III; Snoeyink, J.; Richardson, J. S.; et al. MolProbity: All-Atom Contacts and Structure Validation for Proteins and Nucleic Acids. *Nucleic Acids Res.* **2007**, *35*, W375−W383.

(54) Richardson, J. S.; Schneider, B.; Murray, L. W.; Kapral, G. J.; Immormino, R. M.; Headd, J. J.; Richardson, D. C.; Ham, D.; Hershkovits, E.; Williams, L. D.; et al. RNA Backbone: Consensus All-Angle Conformers and Modular String Nomenclature (an RNA Ontology Consortium Contribution). *RNA* **2008**, *14*, 465−481.

(55) Correll, C. C.; Munishkin, A.; Chan, Y. L.; Ren, Z.; Wool, I. G.; Steitz, T. A. Crystal Structure of the Ribosomal RNA Domain Essential for Binding Elongation Factors. *Proc. Natl. Acad. Sci. U.S.A.* **1998**, *95*, 13436−13441.

(56) Duarte, C. M.; Wadley, L. M.; Pyle, A. M. RNA Structure Comparison, Motif Search and Discovery Using a Reduced Representation of RNA Conformational Space. *Nucleic Acids Res.* **2003**, *31*, 4755−4761.

(57) Wimberly, B.; Varani, G.; Tinoco, I., Jr The Conformation of Loop E of Eukaryotic 5S Ribosomal RNA. *Biochemistry (Mosc.)* **1993**, *32*, 1078−1087.

(58) Szewczak, A. A.; Moore, P. B.; Chang, Y. L.; Wool, I. G. The Conformation of the Sarcin/Ricin Loop From 28S Ribosomal RNA. *Proc. Natl. Acad. Sci. U.S.A.* **1993**, *90*, 9581−9585.

(59) Wadley, L. M.; Pyle, A. M. The Identification of Novel RNA Structural Motifs Using COMPADRES: An Automated Approach to Structural Discovery. *Nucleic Acids Res.* **2004**, *32*, 6650−6659.

(60) Ogle, J. M.; Carter, A. P.; Ramakrishnan, V. Insights Into the Decoding Mechanism From Recent Ribosome Structures. *Trends Biochem. Sci.* **2003**, *28*, 259−266.

(61) Nissen, P.; Ippolito, J. A.; Ban, N.; Moore, P. B.; Steitz, T. A. RNA Tertiary Interactions in the Large Ribosomal Subunit: The A-Minor Motif. *Proc. Natl. Acad. Sci. U.S.A.* **2001**, *98*, 4899−4903.

(62) Noller, H. F. RNA Structure: Reading the Ribosome. *Science* **2005**, *309*, 1508−1514.

(63) Razga, F.; Koca, J.; Sponer, J.; Leontis, N. B. Hinge-Like Motions in RNA Kink-Turns: The Role of the Second A-Minor Motif and Nominally Unpaired Bases. *Biophys. J.* **2005**, *88*, 3466−3485.

(64) Havrila, M.; Reblova, K.; Zirbel, C. L.; Leontis, N. B.; Sponer, J. Isosteric and Nonisosteric Base Pairs in RNA Motifs: Molecular Dynamics and Bioinformatics Study of the Sarcin−Ricin Internal Loop. *J. Phys. Chem. B* **2013**, *117*, 14302−14319.

(65) Leontis, N. B.; Stombaugh, J.; Westhof, E. Motif Prediction in Ribosomal RNAs Lessons and Prospects for Automated Motif Prediction in Homologous RNA Molecules. *Biochimie* **2002**, *84*, 961−973.

(66) Stombaugh, J.; Zirbel, C. L.; Westhof, E.; Leontis, N. B. Frequency and Isostericity of RNA Base Pairs. *Nucleic Acids Res.* **2009**, *37*, 2294−2312.

(67) Ryu, D. H.; Rando, R. R. Decoding Region Bubble Size and Aminoglycoside Antibiotic Binding. *Bioorg. Med. Chem. Lett.* **2002**, *12*, 2241−2244.

(68) Hobbie, S. N.; Bruell, C.; Kalapala, S.; Akshay, S.; Schmidt, S.; Pfister, P.; Bottger, E. C. A Genetic Model to Investigate Drug-Target Interactions at the Ribosomal Decoding Site. *Biochimie* **2006**, *88*, 1033−1043.

(69) Fox, T. D. Mitochondrial Protein Synthesis, Import, and Assembly. *Genetics* **2012**, *192*, 1203−1234.